Arabian Journal of Chemistry (2020) 13, 4644–4660

King Saud University

Arabian Journal of Chemistry

www.ksu.edu.sa
www.sciencedirect.com

ORIGINAL ARTICLE

Functionalized cellulose-preyssler heteropolyacid bio-composite: An engineered and green matrix for selective, fast and in–situ preparation of Pd nanostructures: synthesis, characterization and application

Sara Saneinezhad [a], Fatemeh F. Bamoharram [a,*], Amir Mohammad Mozhdehi [b], Amir Hossein Sharifi [c], Ali Ayati [d], Mehdi Pordel [a], Javad Baharara [e], Mika Sillanpää [f]

[a] *Department of Chemistry, Mashhad Branch, Islamic Azad University, Mashhad, Iran*
[b] *Department of Civil Engineering, Shahrood Branch, Islamic Azad University, Shahrood, Iran*
[c] *Department of Mechanical Engineering, Mashhad Branch, Islamic Azad University, Mashhad, Iran*
[d] *Department of Chemical Engineering, Quchan University of Technology, Quchan, Iran*
[e] *Department of Biology, Mashhad Branch, Islamic Azad University, Mashhad, Iran*
[f] *Laboratory of Green Chemistry, LUT Chemtech, Lappeenranta University of Technology, Mikkeli, Finland*

Received 16 July 2019; accepted 20 October 2019
Available online 31 October 2019

KEYWORDS

Functionalized cellulose;
Preyssler heteropolyaid;
Pd nanoparticles;
Bio-composite;
Catalyst

Abstract A new and green engineered biocomposite was synthesized by sol–gel method, using different loadings of the Preyssler heterpolyacid (8, 15, 25, 40 and 50 wt%) on the functionalized microcrystaline cellulose surface. For the first time, this two-component polymeric biocomposite used for in-situ catalytic synthesis of Pd nanoparticles with the aim of producing tricomponent nanobiocomposites. Preyssler loading on the functionalized surface, controled the size and shape of Pd nanoparticles, time, and pH of their formation. All biocomposites and nanobiocomposites were characterised by FTIR, XRD, BET, TGA, SEM, EDS and TEM. The SEM analysis for two component polymeric biocomposites confirmed the presence of the Preyssler on the surface of functionalized cellulose. The formation of Pd nanoparticles on the surface, was observed by color changing (yellow to deep brown) and confirmed by UV–visible spectroscopy. The Pd nanoparticles

* Corresponding authors at: Department of Chemistry, Islamic Azad University, Mashhad Branch, Rahnamaee Street, Mashhad, Iran.
E-mail address: fbamoarram@mshdiau.ac.ir (F.F. Bamoharram).

Peer review under responsibility of King Saud University.

Production and hosting by Elsevier

https://doi.org/10.1016/j.arabjc.2019.10.006

formation was fast (2–4 min) for 8 wt% in pH = 2–3 at 80 °C. TEM analysis illustrated the spherical Pd nanoparticles with a size of 5–20 nm, at the lowest loading of Preyssler, and rod shapes with a size of 30–40 nm at the highest loading. The obtained nanobiocomposite exhibited high catalytic activity for the decolourisation of tartrazine, as a model of dyes pollutant in the industry with high degradation efficiency. The catalytic reactions were extended with other azo dyes including methyl orange and rodamine B.

1. Introduction

Engineered and functionalized biopolymers have gained much attention for their numerous applications, with improvement of various types of products and commercialization of products. In addition, due to their properties and high potentials, these novel materials have become highlighted worldwide.

For this reason, in the world of green chemistry, bio-based polymers have attracted much attention from researchers in a wide range of fields because of their eco-friendliness, non-toxicity, biodegradability, cost effectiveness and renewability. Along this line, the synergic combination of green and eco-friendly organic and inorganic polymers produces novel hybrids with unique improved properties, such as stiffness, permeability, crystallinity and thermal stability, high exchange capacity and selectivity (Wight and Davis, 2002; Hoffmann et al., 2006; Sanchez et al., 2011). Using biopolymers in these organic/inorganic hybrids leads to the improvement of their stability and mechanical properties as well as their biodegradability. In this regard, the application of cellulose, as a green biopolymer and organic polymeric material for the fabrication of biocomposites, is a rapidly emerging area and the subject of scientific attention (Nabi and Naushad, 2008; Viswanathan and Meenakshi, 2010). The microcrystalline cellulose is an especially attractive organic biopolymer because of its potential advantages such as low cost, renewability, biodegradability, good mechanical properties, availability, simple chemical modification and capacity to bind with inorganic materials (Mishra et al., 2009; Liang et al., 2010). Using cellulose as a matrix for the heteropolyacids as green and eco-friendly inorganic polymers, eventually leading to the synthesis of green composites.

Solid heteropolyacids (HPAs) are a well-known class of green polymeric materials with respect to their non-corrosiveness, safety, quantity of waste and separability. They are composed of the early transition metal cations, M (most commonly W, Mo and V) and a central heteroatom, X (Si, P, Ge, etc.) (Ganapathy et al., 2002). HPAs, with unique properties have been widely used as environmentally homogeneous and heterogeneous catalysts due to their stability and nontoxicity characteristics (Khadempir et al., 2015; Khadempir et al., 2016; Bamoharram et al., 2014; Ayati et al., 2016b; Ayati et al., 2014; Ayati et al., 2015). They catalyse the reactions as surface type, bulk type I, and bulk type II. A literature survey shows that considerable recent research interests have been focused on the development of novel organic–inorganic composites of HPAs and their applications in different reactions (Tripathi and Shahi, 2011; Ayati et al., 2016a). They are also able to be used as heterogeneous surface catalysts, energy supplier, and biodiesel production (Zhang et al., 2016; Ren et al., 2015; Genovese and Lian, 2015). Preyssler acid is a type of HPA that involves a cyclic assembly of five PW_6O_{22} units, each derived from the spherical Keggin anion, $[PW_{12}O_{40}]^{3-}$, by the removal of two sets of three corner-sharing WO_6 octahedron. This structure consists of five PO_4 tetrahedron surrounded by 30 WO_6, connected to each other by edge and corner-sharing oxygens (Bamoharram et al., 2006). The objective of this work is designing of an organic–inorganic polymeric biocomposite including functionalized microcrystalline cellulose (FC) and Preyssler heteropolyacid for the in-situ catalytic preparation of Pd nanoparticles (PdNPs) on the surface to the formation of nanobiocomposite as surface heterogeneous catalysts. Supported Pd heterogeneous catalysts as well as other organic and inorganic supports loaded with nanoparticles have been attracted great attention in various fields of chemistry due to their high potential for economic considerations (Opanasenko et al., 2014, Cheng et al., 2013, Lu et al., 2013, Li et al., 2012, Chang et al., 2012, Liu et al., 2012). One of the methods for preparing supported Pd catalysts are coordinating Pd with pregrafted functional groups on the surface of support (Sheldon and Van Bekkum, 2007). The used supports so far are including carbon materials, metal oxides, porous silicate, molecular sieves, silica materials, synthetic polymers, and biopolymers, especially cellulose (Polshettiwar and Molnár, 2007; Djakovitch and Koehler, 2001; Klingelhöfer et al., 1997; Guibal, 2005). The extensive applications of cellulose-based functional materials in various fields were investigated by many researchers (Li et al., 2018).

Most progress was made on the fields of biological applications, water treatment, sensors, and reinforcing agents with only a few reports on energy storage materials and Pickering emulsion stabilizer. Recently, several papers have described the immobilization of Pd on the surface of nanocellulose using different strategies and precursors to obtain cellulose-based functional materials and studied their catalytic activity (Rezayat et al., 2014; Zhou et al., 2012; Wu et al., 2013; Li et al., 2017; Zhang et al., 2018). In addition, Peipei Zhou et al. investigated the preparation of the targeted Pd/Bacteria cellulose with higher Pd loading and studied its applicability in Heck reaction as catalyst (Zhou et al., 2012).

Zeyneb Jebali and coworkers used cationic cellulose nanofibrils as a support for the growth and the immobilization of Pd NPs and tested it as a catalyst for the Suzuki coupling reactions (Jebali et al., 2018). Facile synthesis of palladium and gold nanoparticles by using dialdehyde nanocellulose as template and reducing agent was reported by Kaitao and coworkers (Zhang et al., 2018). Moreover, Hiroaki Ito et al. prepared oxidation-treated nano-sized fibrillated cellulose/AgNPs nanobiocomposite and investigated their mechanical and functional properties (Ito et al., 2018).

We found that the synthesis of nanostructures using biopolymers assisted by Preyssler acid has been unexplored, which is a good reason for conducting the present research. In continuation of our earlier researchs on the applications of Preyssler acid in the synthesis of nanostructures (Ayati et al., 2012; Tanhaei et al., 2017), it was valuable to us to investigate the role of Preyssler in combination with cellulose biopolymer to the formation of green nanobiocomposites as an effective bifunctional heterogeneous catalyst. A few reports have described the green synthesis of carboxymethyl cellulose-supported Pd nanoparticles by the direct reduction of palladium species with carboxymethyl cellulose as a green reductant (Wu et al., 2013; Chen et al., 2014). In one reaction, the cellulose nanocrystal-supported Pd nanoparticles were synthesized for a long time (12 h) at a high temperature (100 °C) (Wu et al., 2013). In another reaction, the cellulose microencapsulated Pd NPs were synthesised in a cellulosic ionic liquid solvent (Chen et al., 2014). Therefore, regarding the great success of cellulose as support for heterogeneous catalyisis, (Rajender Reddy et al., 2006; Cirtiu et al., 2011; Xu et al., 2008; Yang et al., 2011; Klemm et al., 2005) catalytic activity of NPs/cellulose composites (Zhou et al., 2012; Zhang et al., 2018; Bhardwaj and Paul, 2016) and our interest in developing catalytic activity of supported- Preyssler heteropolyacid, the main goal for this work is synthesis and characterization of functionalized cellulose-Preyssler (FCP) as a green and reactive polymeric matrix for selective, fast and in–situ catalytic preparation of Pd nanostrucures (FCP/Pd). Moreever, in order to study the synergistic effect of cellulose, Preyssler and the prepared PdNPs on the surface, the decolourisation of azo dyes performed as a test reaction to estimate the catalytic activity of them. Interestingly FCP/Pd showed higher catalytic activity rather than each of FC and FCP alone. This observation indicates that this catalytic activity can be extended to the other azo dyes as well as other catalytic reactions. To the best of our knowledge, this is the first time that Preyssler is immobilized on the FC and used for in-situ catalytic synthesis of PdNPs on its surface, for obtaining a tricomponent nanobiocomposite to use as green, recyclable and new nano catalyst for decolorization of azo dyes.

2. Materials and methods

2.1. Materials

Preyssler heteropolyacid was prepared by passage of a solution of the potassium salt in water through a column (50 cm^{-1}) of Dowex resin in the H^+ form and evaporation of the elute to dryness under vacuum (Bamoharram et al., 2006). Microcrystalline cellulose (Cotton linters powder), ethanol (99.5% w/w), concentrated nitric acid (65% w/w); ammonia aqueous solution (25% w/w), tetraethyl orthosilicate (98% w/w), 3-aminopropyltriethoxysilane (95% w/w), azo dyes and palladium chloride (purity 99%) were purchased from Sigma–Aldrich Company and used as received.

2.2. Methods

2.2.1. Preparation methods

2.2.1.1. Synthesis of functionalized cellulose-Preyssler biocomposites (FCP). An aqueous solution contained of tetraethyl orthosilicate (37.5 mL), 3-aminopropyltriethoxysilane (1.55 mL) and ethanol (20.5 mL) was acidified with a few drops of concentrated nitric acid and then nitric acid (800 μL) was added again. After 50 min of stirring, dilute ammonia was added in small portions, stirred for more 15 min, followed by the gradual addition of microcrystalline cellulose (1.5 gr) and left to stir for a short time. Then, a solution of Preyssler HPA in different amounts including 8, 15, 25, 40 and 50 wt% was added and the suspension was allowed to stir for 15 min. The obtained white solid was separated using centrifugation at 4000 rpm for 20 min, washed several times with water and dried at 60 °C.

2.2.1.2. Synthesis of FCP/Pd NPs nanobiocomposites. For a typical synthesis of PdNPs, 10 mL of $PdCl_2$ solution (1.5 mM) and FCP (1.0 wt% in 10 mL H_2O), as a catalyst, were stirred and sodium hydroxide was dropwise added into the reaction mixture to adjust the pH. Then, the mixture was heated in a water batch until 70–80 °C. PdNPs were synthesised at pH = 2–6 within 2–20 min. At equal time intervals, the solutions were analysed by a UV–Vis spectrophotometer to follow the synthesis processes.

2.2.1.3. Catalytic activity study. Typically, 15 mg of catalyst (FCP/Pd NPs with 8 wt% Preyssler loading) were added to the test tubes containing 10 mL of tartrazine solution (20 mg/L) and Preyssler acid (6 mM) and stirred on a shaker. At given time intervals, all of the mixtures were immediately filtered by using syringe filters and the tartrazine concentration of the filtrate was analysed by a UV–Vis spectrophotometer at λ_{max} = 420 nm.

2.3. Characterization

Infrared absorption spectra were recorded on a VERTEX-70 infrared spectrometer in KBr pellets using the ATR method. The phase components and crystallinity of composites were examined by their X-ray diffraction data which were collected using a PANalytical Empyrean powder diffractometer by Cu-Kα radiation. Data were collected by the step counting method in the 2 tetha range of 10–45o. Circular pellets were prepared for analysis by pressing the samples at 50 MPa during 2 min. The morphology and size of nanoparticles were obtained by transmission electron microscope (Hitachi HT7700 instrument). For TEM analysis, one drop of the metal nanobiocomposite suspension was gently placed on a carbon-coated Cu grid, hydrophilized via plasma discharge, and dried at room temperature. The Hitachi SU3500 scanning electron microscope at 25 kV, using gold coated samples was used for the analysis of surface morphology of prepared composites. The instrument was equipped with the EDX model of Thermo Scientific UltraDry SDD (dual detector) for elemental analysis determination. Specific surface area and pore size distributions (BET analysis) were determined through nitrogen (N_2) adsorption–desorption approach using Micromeritics Tristar II plus instrument at 77.35 K in the relative pressure (P/P_0) range of 10–6–1. Barret, Joyner and Halenda (BJH) method was used for the calculation of pore volume distribution. Thermogravimetric (TGA) analysis was carried out under nitrogen atmosphere in the temperature range of 20–800 °C and heating rate of 5 °C min^{-1} using a Netzsch Thermo-Microbalance

TG 209 F1 Iris. Moreover, a JASCO V-670 UV–vis spectrophotometer (Japan) was employed to study the PdNPs formation and also the concentration measurement of tartrazine azo dye.

3. Results and discussion

The combination of cellulose with inorganic polymers and metal NPs to design multifunctional nanobiocomposites is an interesting approach to extend the applications of these materials. This combination is an important but less exploited strategy to prepare multifunctional nanobiocomposites. Nowadays, the preparation of multifunctional nanobiocomposites have been performed in several ways to improve the performance of nanobiocomposites (Pinto et al., 2012; Azetsu et al., 2011; Liu et al., 2011; Zou et al., 2012; Irvin et al., 2019; Yu et al., 2016; Fortunati et al., 2012a,b). These methods require harsh or complicated conditions, long reaction times, hard work-up procedures and lead to wastes and high cost. Compared to the literature, we have developed an alternative and simple procedure for the surface synthesis of a new and green nanobioocomposite, cellulose/Preyssler/PdNPs, as an eco-friendly, inexpensive and efficient catalyst in water treatment. High yields, short reaction times, simplicity of operation and easy work-up procedure are some advantages of this protocol.

3.1. Characterisation of FCP in different loadings of Preyssler

The green biocomposites FCP, were synthesised by cellulose biopolymer containing silica modified with propylamino groups and Preyssler HPA. The protonated amino groups on the surface of silica-functionalized cellulose (SFC) can easily interact with Preyssler acid through an electrostatic interaction to prepare green and novel organic/inorganic biocomposite. Different amounts of Preyssler were added to the aqueous SFC including 8%, 15%, 25%, 40% and 50%. By several washings of the synthesized biocomposites, less than 2–3%

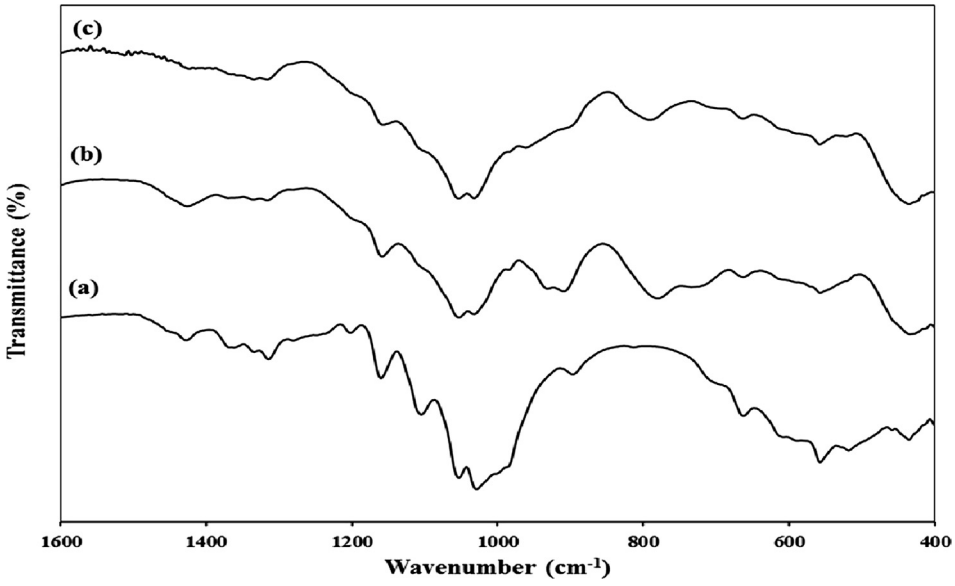

Fig. 1 FTIR spectra of (a) cellulose, (b) FCP, and (c) Preyssler acid.

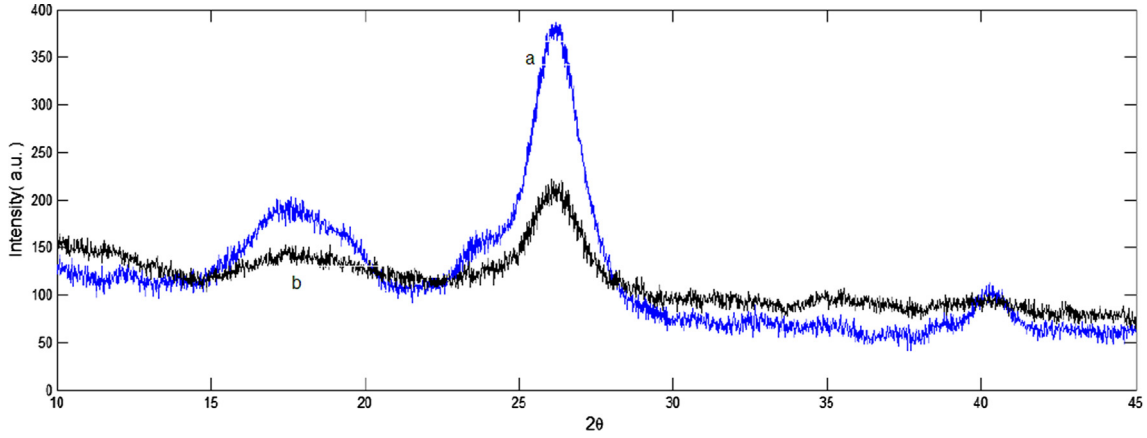

Fig. 2 X-ray patterns of (a) cellulose and (b) FCP.

of the Preyssler was extracted into the solvent. The prepared biocomposites of FCP were characterised by FTIR, XRD, BET, TGA, SEM and EDS analysis. The FTIR spectra of cellulose, Preyssler and FCP are presented in Fig. 1. The results revealed that the peaks of Preyssler acid appeared in the spectrum of FCP compared to that of raw cellulose, but the spectra of biocomposites FCP with different loadings of Preyssler were nearly identical to each other and no differences were observed due to the different loadings. The FTIR spectrum of cellulose (Fig. 1a) presents several characteristic bands, due to the C—O—C and C—O—H stretching vibrations in the range of 400–1400 cm $^{-1}$.

In the spectrum of FCP (Fig. 1b), an additional band appeared at 788 cm^{-1} assigned to (Si—O—Si). The band expected at about 1080 cm^{-1} (Si—O—Si) was overlapped with the bands of cellulose in the same spectral region. In addition, the sharp band at 1480 cm^{-1} is due to nitrate anions. On the other hand, most of the absorption bands of Preyssler HPA were masked by modified cellulose matrix in 600–1200 cm^{-1}. Preyssler's structure gives rise to four types of oxygen that are responsible for the fingerprint bands of the Preyssler anion between 1200 and 600 cm^{-1}. The characteristic bands of the Preyssler structure, $[NaP_5W_{30}O_{110}]^{14-}$ are three bands due to P-O stretching at 1163 cm^{-1}, 1079 cm^{-1}, and 1022 cm^{-1}, two bands attributed to W-O-W at 941 cm^{-1} and 913 cm^{-1}, a band at 757 cm^{-1} corresponding to W = O and a band at 536 cm^{-1} due to P-O bending. These bands can shift, weaken, strengthen, or mask in different conditions. In Fig. 1b, compared with the initial Preyssler's structure (Fig. 1c), the bands arising from the synthesized biocomposite changed obviously either in intensity or in position. Our findings showed that many of the vibrational bands of Preyssler have blue or red shifted and many of them have masked with cellulose and silica. This means that many of the bonds were strengthened and

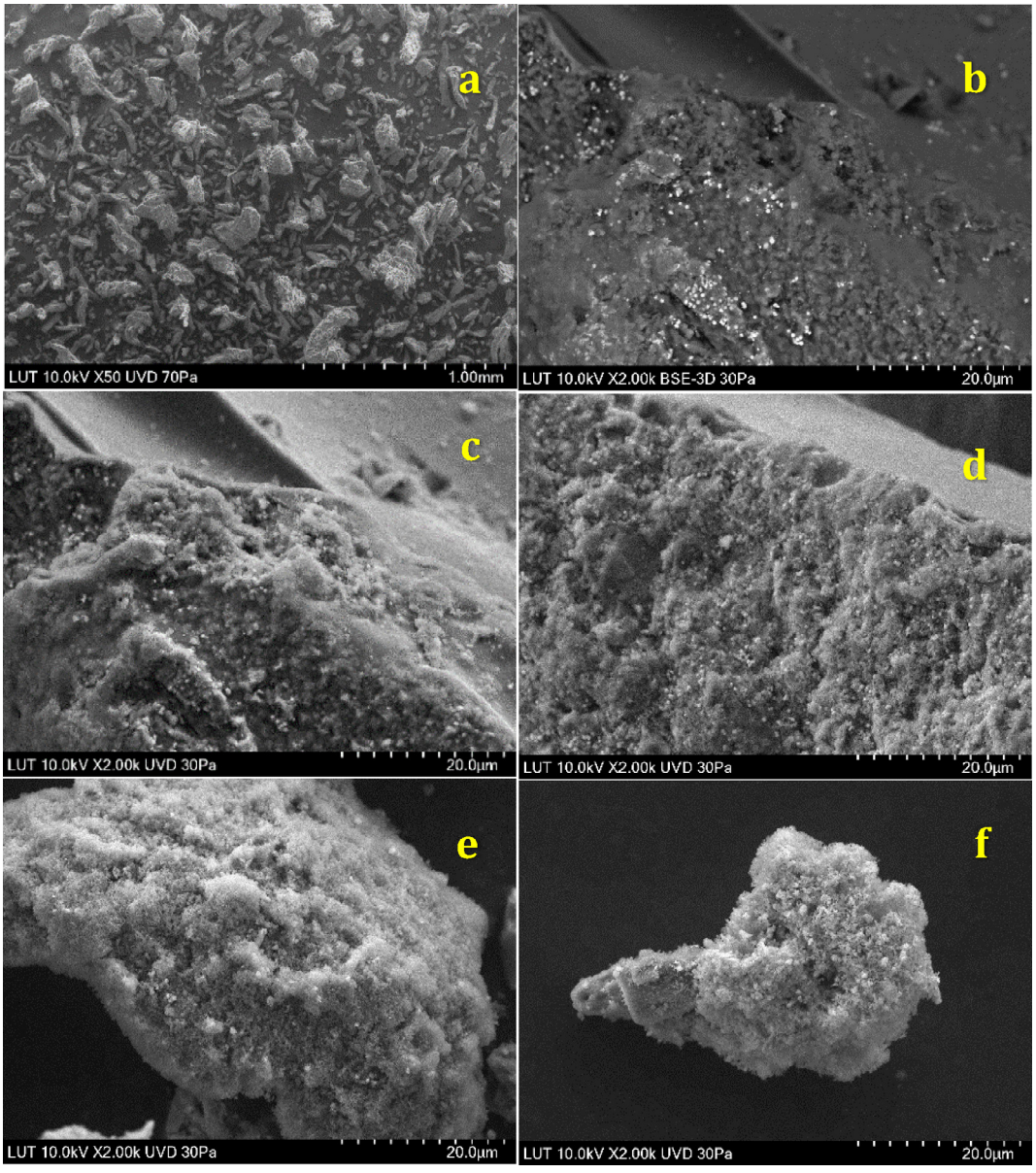

Fig. 3 SEM images of FCP in different loadings of Preyssler: (a) micro crystalline cellulose, (b) 8%, (c) 15%, (d) 25%, (e) 40%, (f) 50%.

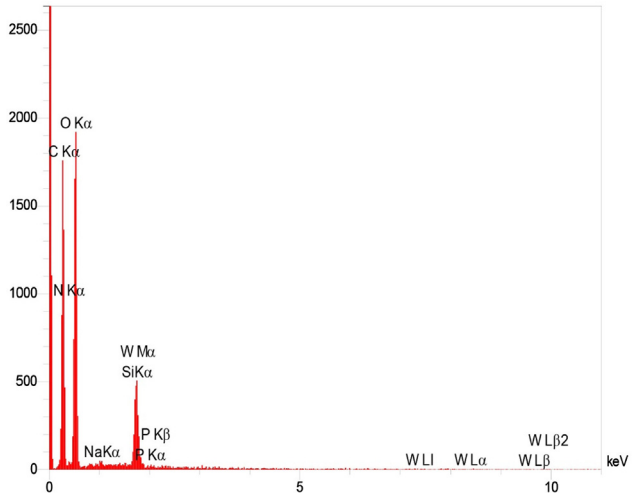

Fig. 4 EDS elemental mapping images for FCP.

the others were weakened. As it can be seen, there is a significant shift in the W-O-W vibrations from 941 to 959 cm^{-1} and the P-O bands are overlapped by that of cellulose and silica materials. The characteristic band in 913 cm^{-1} is unchanged, but the W = O band along with the P-O bending bands are overlapped by that of functionalised cellulose. With respect to the PO_4 tetrahedrons vibrate almost independently from the rest of the anion, the significant blue shift of 18 cm^{-1} in the W-O-W vibrational mode suggests that Preyssler interacts strongly with the modified surface and binds to it by the oxygen atoms in the W-O-W positions. These observations indicate that an interaction between Preyssler's anion and support mostly caused the distortion of anion and thus substantially not only weakened the IR vibrations covered up by the background, but also caused some displacements in some bands. XRD analysis of cellulose and FCP are shown in the Fig. 2. The X-ray diffractograms show the reflections around $2\theta = 18°$ and 26° related to the 101 and 002 faces, assigned to the cellulose. X-ray patterns in Fig. 2b shows FCP presented the non-resolved reflections from the 101 planes around 18° and the reflection from the 002 plane at about 26°. It means, the basic structure of cellulose was preserved in the hybrid polymers. The peaks of FCP in Fig. 2b are weaker than the initial cellulose, due to the introduction of Preyssler heteropolyacid into the structure of amine-functionalized cellulose. It is suggested that after modification by reagents with different amine groups on the surface, the functionalized cellulose may has a lower steric hindrance and this resulted in a higher loading content of Preyssler and more decrease in characteristic peaks of cellulose. In fact, such behaviour is expected for the heteropolyacids when immobilized on different supports. The surface morphology of FCP biocomposites with different Preyssler loadings were examined by SEM analysis and their

Table 1 BET results for FCP with different loadings of Preyssler.

	Loading of Preyssler on functionalized cellulose (wt%)				
	8	15	25	40	50
BET surface area	23.7909 m^2/g	17.5488 m^2/g	5.2393 m^2/g	1.9144 m^2/g	0.5342 m^2/g
Pore size – BJH Adsorption average pore width (4 V/A)	136.308 Å	139.785 Å	208.575 Å	465.422 Å	600.379 Å
Pore size – BJH Desorption average pore width (4 V/A)	135.908 Å	140.996 Å	201.546 Å	368.134 Å	434.755 Å

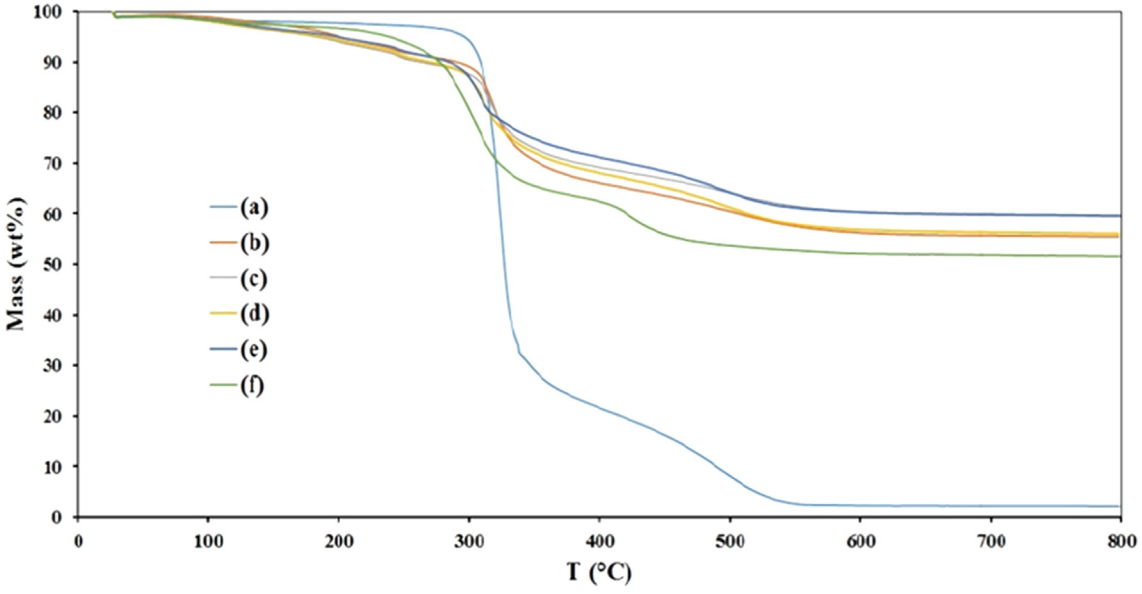

Fig. 5 Thermogravimetric curves of (a) initial cellulose, and FCP with the Preyssler loadings of b) 8%, (c) 15%, (d) 25%, (e) 40% and (f) 50%.

images are shown in Fig. 3. As can be seen in these Figures, obviously they show the coating of Preyssler on the surface of functionalized cellulose, in which the roughness of surface was reduced in the higher loading of Preyssler.

The EDS analysis confirmed the presence of C, O, N and Si in FCP as well as the presence of P, Na and W attributed to the presence of Preyssler HPA (Fig. 4). Both the SEM and EDS analyses demonstrated the highly surface coverage of cellulose with Preyssler, although some regions might be only partially coated with modified silica. The elemental composition of W in the FCP with different loading of Preyssler was 27.3% for the lowest loading and increased to 52.3% for the highest loading. On the other hand, the BET analysis was performed for FCP with different loadings of Preyssler acid. The results are summarized in Table 1 which show that the surface area of biocomposites decreases by the addition of Preyssler loading, which might be due to more pores being blocked.

The TGA results for biocomposite FCP with different loadings of Preyssler are shown in Fig. 5. Interestingly, compared to microcrystalline cellulose, thermal decomposition is varied with the loading of the Preyssler. Thermal decomposition of cellulose typically leads to a solid residue (char), high boiling volatiles (tar) and gaseous products. These pathways are including the dehydration of cellulose to anhydrocellulose, which further decomposes to gases and char, or the depolymerisation of cellulose at somewhat high temperatures producing tar (mainly levoglucosan), and combustible gases. The additives strongly modify the decomposition process of cellulose, enhancing the char and reducing tar formation. In this work, the addition of Preyssler to cellulose shifts the whole process dehydration and depolymerisation to a lower temperature. The fact that levoglucosan was not well detected in the high boiling products, could be explained by the presence of the Preyssler interfering with depolymerisation. The thermogeravimetric curves of FCP with different Preyssler loadings have almost the same trend and show 3 steps for losing the weight. The first step is attributed to moisture release at about 122 °C (2.5%). The second step starts at 126–300 °C and is related to the decomposition of the amino sections and nitrate anions (10%). In the third step in the range of 300–800 °C, the 25–30% weight loss is due to cellulose decay. From the thermograms, it is suggested that the weight decay of cellulose in all biocomposites is nearly the same.

3.2. In-situ catalytic synthesis and characterisation of PdNSs in the presence of FCP to prepare the green nanobiocomposites

The prepared FCP has been checked, as a promising green catalyst, with a different loading of Preyssler for the preparation of PdNPs. The formation of PdNPs on the surface of FCP was observed by colour change from yellow to deep brown in solution, and confirmed by UV–visible spectroscopy step by step. The visual colour changed from yellow to deep brown and was observed in the presence of FCP with keeping the initial concentration of $PdCl_2$ constant at 1.5 mM. Interestingly, the speed and pH of the formation for PdNPs were varied as a function of increasing Preyssler loading in FCP. The PdNPs formation was very fast (2–4 min) in loading of 8 wt% in the pH range of 2–3 at 80 °C. Our observations showed that the colour change of $PdCl_2$ solution was started from pH = 2 which indicated the formation of PdNPs. During the mentioned pH range, suddenly PdNPs formed as snowflakes and solution filled with brown nanoparticles rapidly that were locally decorated on the surface of FCP to form FCP/Pd nanobiocomposites. PdNPs deposited at the bottom of vessel and a colourless solution was obtained immediately. Fig. 6 shows the preparation process of nanobiocomposite, step by step. These observations were different at the higher loading of Preyssler. For higher loadings PdNPs were formed in longer times and different pH. Also the time of nanobiocomposite

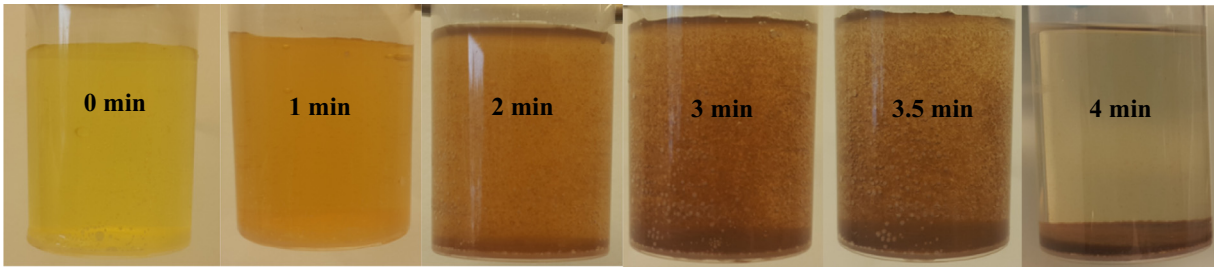

Fig. 6 Catalytic formation of nanobiocomposite FCP/Pd (pH = 2–3, 8%).

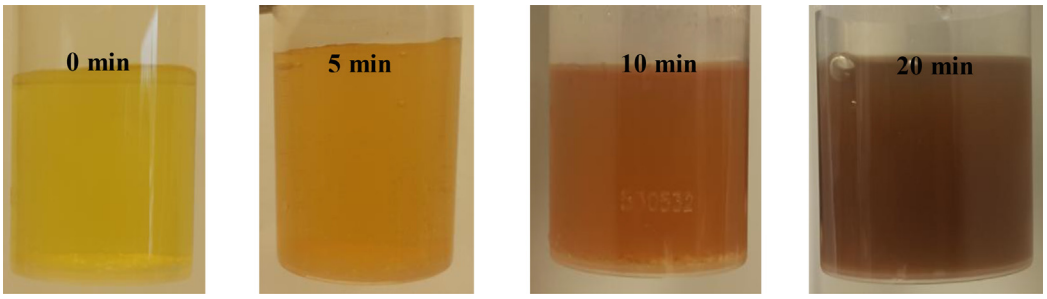

Fig. 7 Catalytic formation of PdNPs in the presence of FCP with other Preyssler loadings.

Table 2 The formation conditions of nanobiocomposites in the presence of FCP.

Entry	Preyssler loading (%)	Time (min)	pH
1	8	2–4	2–3
2	15	10	1.3–4
3	25	10	2–5
4	40	15	2–5.7
5	50	20	1–5.5

deposition increased to several hours. The formation of FCP/PdNPs in the presence of FCP at higher loadings is illustrated in Fig. 7 and their conditions are presented in Table 2.

In a blank reaction, the formation of PdNPs was checked in the presence of the FC without Preyssler loading and no formation of nanostructures was observed. It demonstrates the reductant role of Preyssler catalyst in the biocomposite FCP. All these results suggest that Preyssler acts simultaneously as a linker and reductant catalyst in the presence of biocomposite

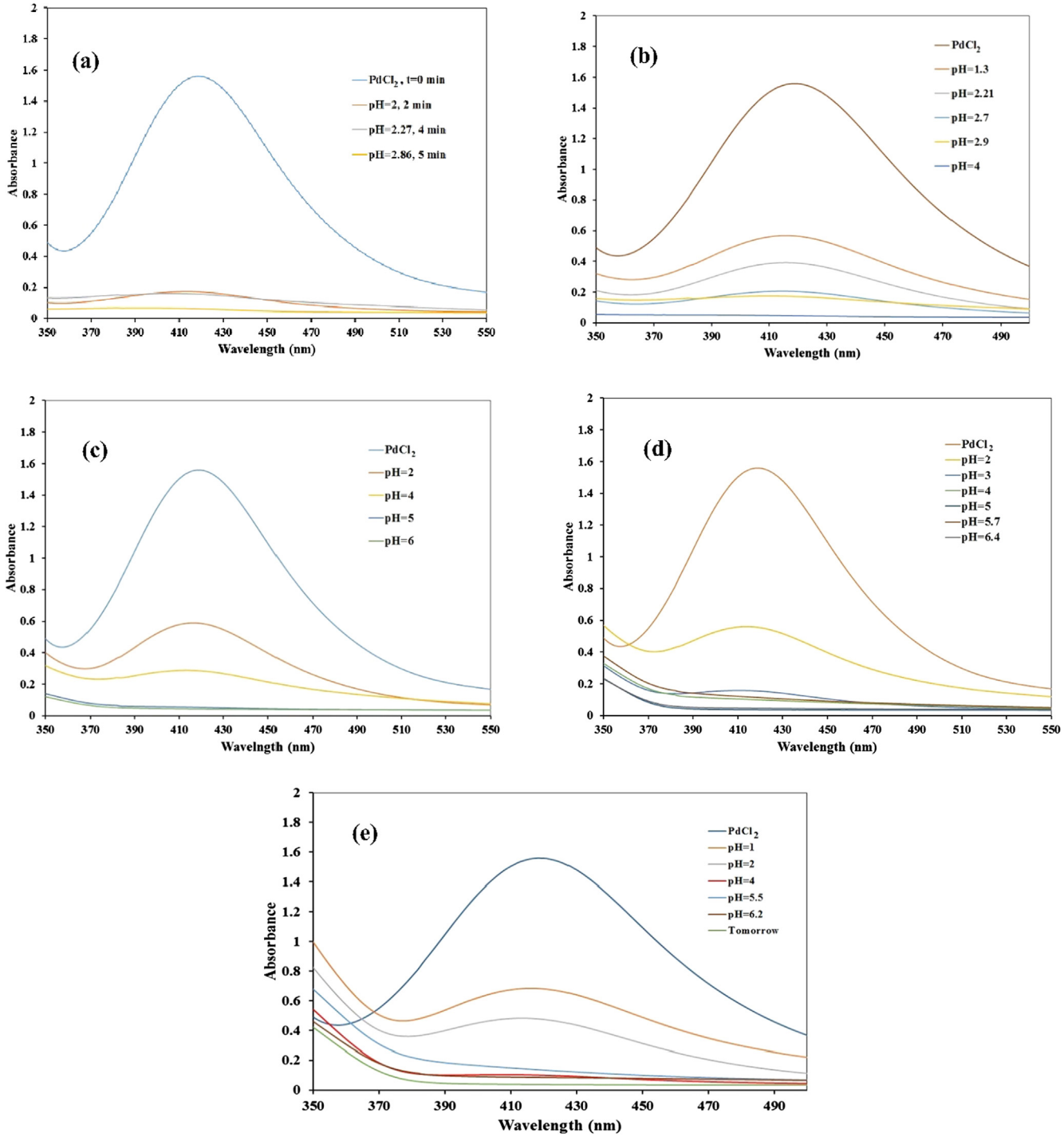

Fig. 8 UV–visible spectra of PdNPs formation with different loadings of Preyssler: (a) 8%, (b) 15%, (c) 25%, (d) 40%, and (e) 50%.

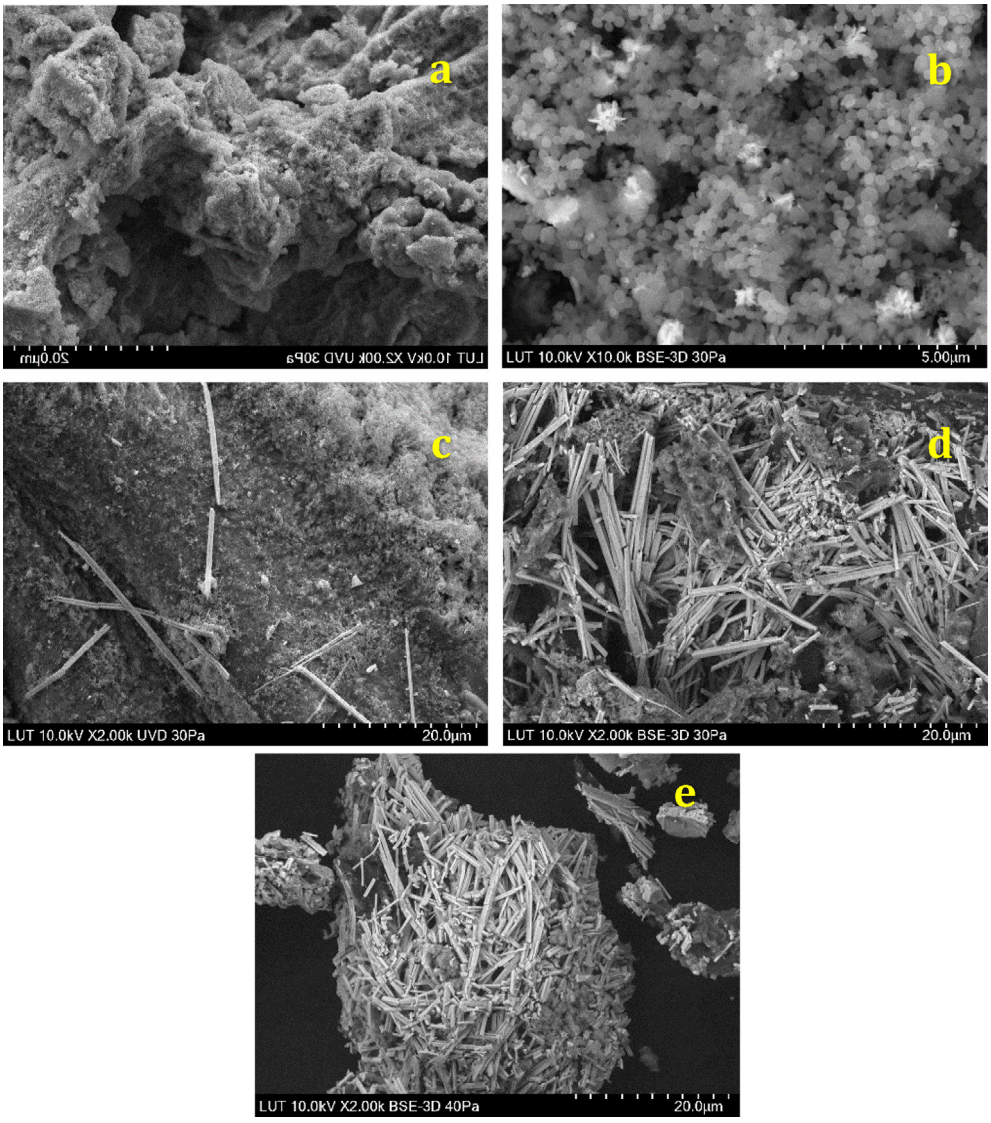

Fig. 9 SEM images of FCP/Pd nanobiocomposites in different Preyssler loadings: (a) 8%, (b) 15%, (c) 25%, (d) 40%, (e) 50%.

with 8 wt% loading (Fig. 6), while it serves as linker, reductant, and stabilizer in higher loadings. A probable explanation for this behaviour may be attributed to the leaching of Preyssler in higher loadings, which can lead to releasing the Preyssler in the solution and stabilizing of the non-decorated PdNPs. This phenomenon strongly inhibited the deposition of PdNPs on the surface of the FCP biocomposite. This is a common occurrence in the polyoxometalate catalysis when immobilized on different supports.

In a systematic study, the process of PdNPs synthesis was checked by UV–vis spectroscopy. Fig. 8 shows the Uv–vis spectra of PdNPs formation as a function of pH. The absorption band at 428 nm is related to the charge transfer transition between Pd(II) and chloride ions. The disappearance of this absorption band along with a visual colour change confirmed the reduction of the Pd (II) ions to Pd(0).

Pd(II) could reduce completely in the presence of biocomposite FCP with the loading of 8% and a brown nanobiocomposite formed at the bottom of vessel rapidly. The supercant was completely clear in just 4 min (as can be seen in Fig. 6). Increasing the Preyssler loadings further to 50% resulted in longer times to the formation of PdNPs up to approx. 30 min. As can be seen, the formation depends on the loading of Preyssler and the pH of the solution. The Preyssler anion provides highly distributed charged surfaces, which is ideal for binding the metal ions from their aqueous precursor solutions. The higher Pd NPs loading in the 8% is related to an increased number of sites for binding Pd(II) ions.

FTIR of the prepared novel nanobiocomposites FCP/PdNPs with different loadings of Preyssler were identical to each other as well as FCP as shown in Fig. 1.

Furthermore, the morphologies of the synthesised nanobiocomposites were checked by SEM equipped with EDS. Fig. 9 shows the SEM micrographs of the FCP/Pd nanobiocomposites with different loadings of Preyssler. These images show the PdNPs are cloudy and spherical at the low Preyssler loadings, whereas they changed to rod shaped by increasing the loading of Preyssler. In addition, the SEM images clearly indi-

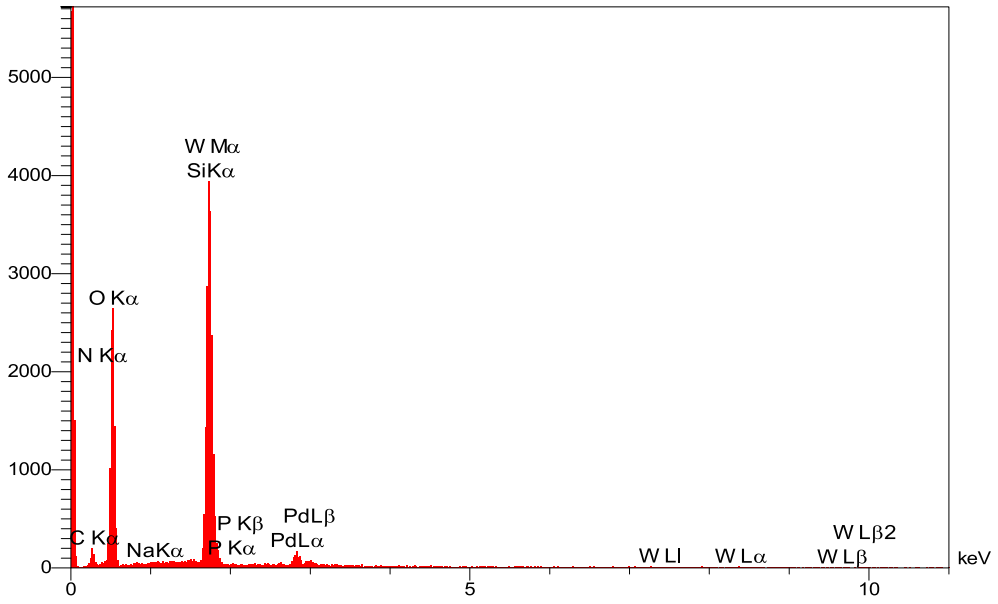

Fig. 10 EDS elemental mapping images for FCP/Pd.

cate that the formation of nanorods starts in the presence of 25 wt% Preyssler and gradually increased until 50 wt% Preyssler loading.

In addition, the EDS analysis of nanobiocomposites showed that C, O, Si, N, W, P, Na and Pd atoms are present in the structure (Fig. 10). Interestingly, wt. % of PdNPs was varied in the range of 3.5–27% with different loadings of Preyssler on the surface of functionalized cellulose.

On the other hand, the formation of PdNPs on the surface of FCP was further characterisized by TEM. Fig. 11 shows the TEM images of the synthesized nanobiocomposites including PdNPs and interestingly confirmed the obtained results from SEM observations (Fig. 9). As can be seen, the PdNPs are spherical in shape at the lowest loading of Preyssler with a size of approx. 5, 15, and 20 nm for 8%, 15%, and 25% loading, respectively. As the loading of Preyssler was gradually increased, a change in morphology was observed from spherical to rod shapes with a size of 30 and 40 nm for 40% and 50% loading. Thus, it is concluded that the sizes and morphologies of PdNPs depend markedly on the amount of loaded Preyssler catalyst on the surface of the functionalized cellulose. It can be suggested that the large interaction of Preyssler with functionalized cellulose could cause robust immobilization on cellulose with high surface density.

In addition, their strong binding with Pd metal could enable it to be an efficient reductant, stabilizer and shape-directing biocomposite for the synthesis of PdNPs with a uniform size and shape as well as allowing for the local synthesis of the PdNPs on the surface of FCP with high density, good dispersion and high stability. At a lower pH, the nucleation process is faster, resulting in smaller PdNPs. The higher content of nanorods formed at higher pH implies that the formation of nanorods is a kinetically controlled process (Lim and Xia, 2011; Cheong et al., 2010). When the growth rate is low, the atom addition is slower than adatom diffusion. This allows for the migration of adatoms on the nanocrystal surface to minimize the total surface energy, leading to the formation of nanospheres (Lim and Xia, 2011; Wang et al., 2015). However, when the growth rate increases by increasing the pH of solution, a faster rate of atomic addition can cause high energy faces grow more quickly than that of low-energy ones, thus creating high-surface-energy nanostructures such as nanorods. However, no one has used Preyssler-cellulose biocomposite for controlled, shape-directing and surface in-situ synthesis of PdNPs to the formation of green nanobiocomposites. However, parameters capable of influencing nanoparticle size may be different. In wet-chemistry approaches, concentrations in liquid phase, temperature, and presence or absence of surface modifiers, are perhaps the most common and known parameters. On the other hand, the synthesis method, controlling the pH, concentrations and additives can change the grain size. Reaction time, especially the time for the condensation process, power of reducing agents, the use of a capping agent or surfactant, and type of precursors are also critical.

The time for Pd NPs to precipitate from solution was investigated. It can be seen from Figs. 6 and 7 and table 2 that time to precipitate decreased over increasing pH (2–5.7). The data showed that pH plays a very significant role in size of nanoparticles as well as the loading of them. One of the prominent characteristics of nanoparticles are that they tend to float in solution and they need much longer time to be precipitated in as much as the gravitation force exerting them is very small, or even almost negligible (Baruah and Dutta, 2009). It was hypothesized that by varying the pH conditions, the loading and size of the particles obtained would also be varied, and this would affect the precipitation profile of the Pd nanoparticles. To test above hypotheses, amount of the loading and size of the particles at lower and upper pH (pH 2 and pH 5.7) were measured by TEM. Results showed that the size of nanoparticles at pH 2 and pH 5.7 were 5–20 nm and 30–40 nm, respectively. It is in agreement with hypotheses above that as pH of the solution increased, the size of the nanoparticle increased as well.

Surprisingly, an increased surface area was observed when the surface area of the FCP/Pd nanobiocomposites (Table 3)

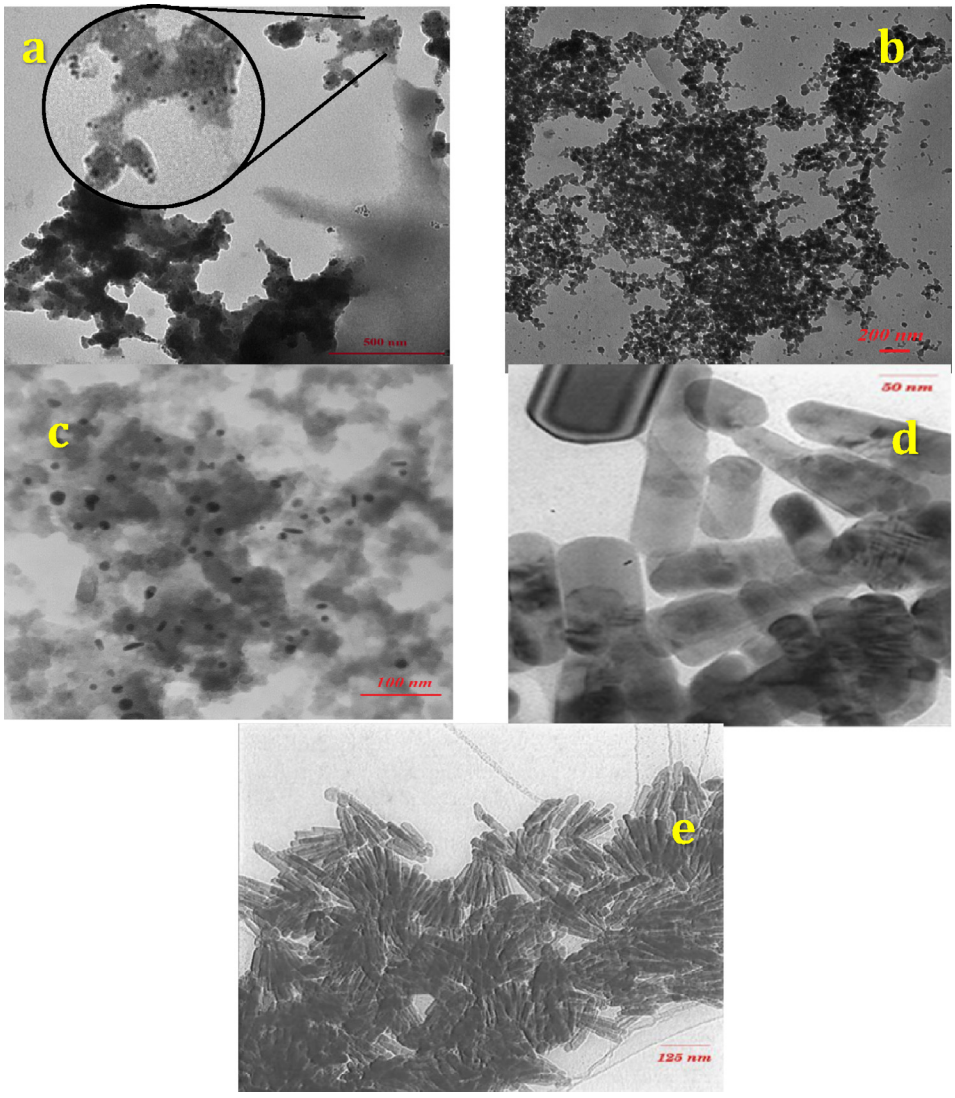

Fig. 11 TEM images of FCP/Pd nanobiocomposites in different Preyssler loadings (a) 8%, (b) 15%, (c) 25%, (d) 40%, (e) 50%.

Table 3 BET results of nanobiocomposites FCP/Pd with different loadings of Preyssler.

Preyssler loading amount (g)	8%	15%	25%	40%	50%
BET surface area (m^2/g)	27.4470	19.2651	17.8993	11.0540	8.2310
Pore size – BJH Adsorption average pore width (4 V/A) (Å)	87.597	126.395	127.061	72.984	263.788
Pore size – BJH Desorption average pore width (4 V/A) (Å)	89.854	136.839	128.949	73.877	200.362

was compared to that of FCP (Table 1). The increase in the surface area can be due to the high dispersion of PdNPs on the FCP, but no block on pores.

Moreover, the TGA results of prepared FCP/Pd nanobiocomposites, as shown in Fig. 12, illustrate that the approximate quantification of cellulose content in all FCP/Pd nanobiocomposites is about 30–42%. There is no significant difference between the thermal decomposition of FCP and FCP/Pd. It is suggested that the dispersion of PdNPs as well as the presence of Preyssler shifts the whole dehydration process and depolymerization to a lower temperature.

3.3. Catalytic removal of tartrazine dye using nanobiocomposites FCP/Pd

Tartrazine, which is an anionic azo dye, has been chosen for this study due to its extensively use in the food, drugs and cosmetics industries (Tanaka, 2006), as a colouring agent. It has high stability against biodegradation and conventional wastewater treatment procedures and causes more allergic and intolerance reactions than other azo dyes. It also has high solubility in water and most people are extremely sensitive to tartrazine, as it can cause breathing difficulties, asthma, urti-

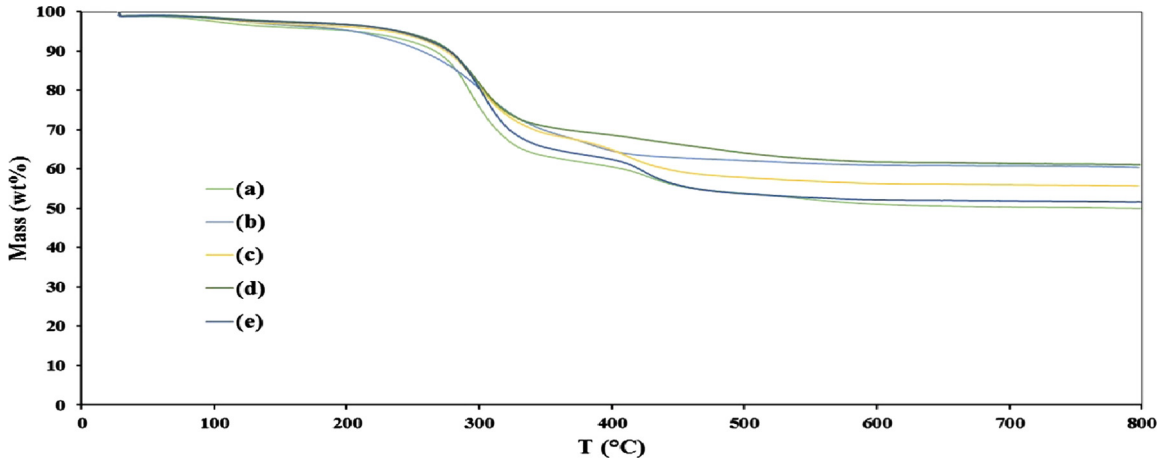

Fig. 12 Thermal decomposition of FCP/Pd with a different Preyssler loading of (a) 8%, (b) 15%, (c) 25%, (d) 40%, (e) 50%.

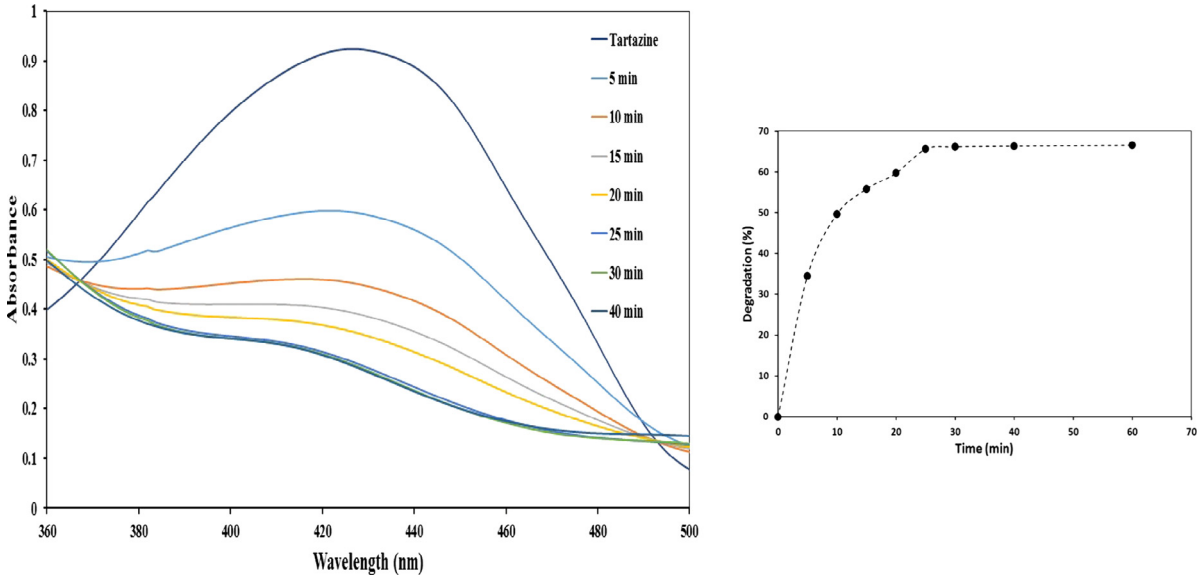

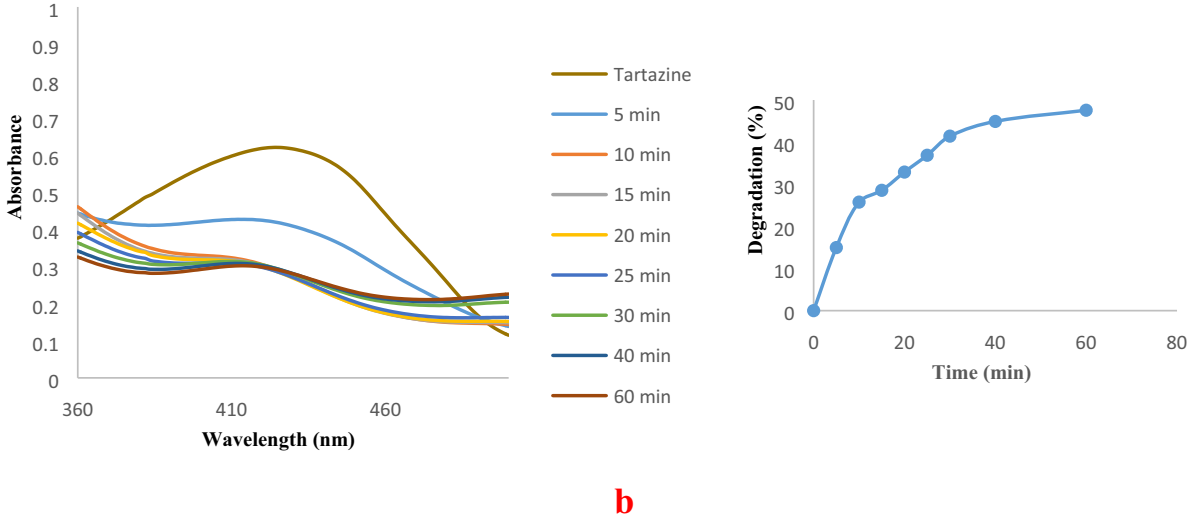

Fig. 13 UV–visible spectra of (a) tartrazine catalytic decolourisation in the presence of FCP/PdNPs as spherical, and (b) tartrazine catalytic decolourisation in the presence of FCP/PdNPs as rod shape.

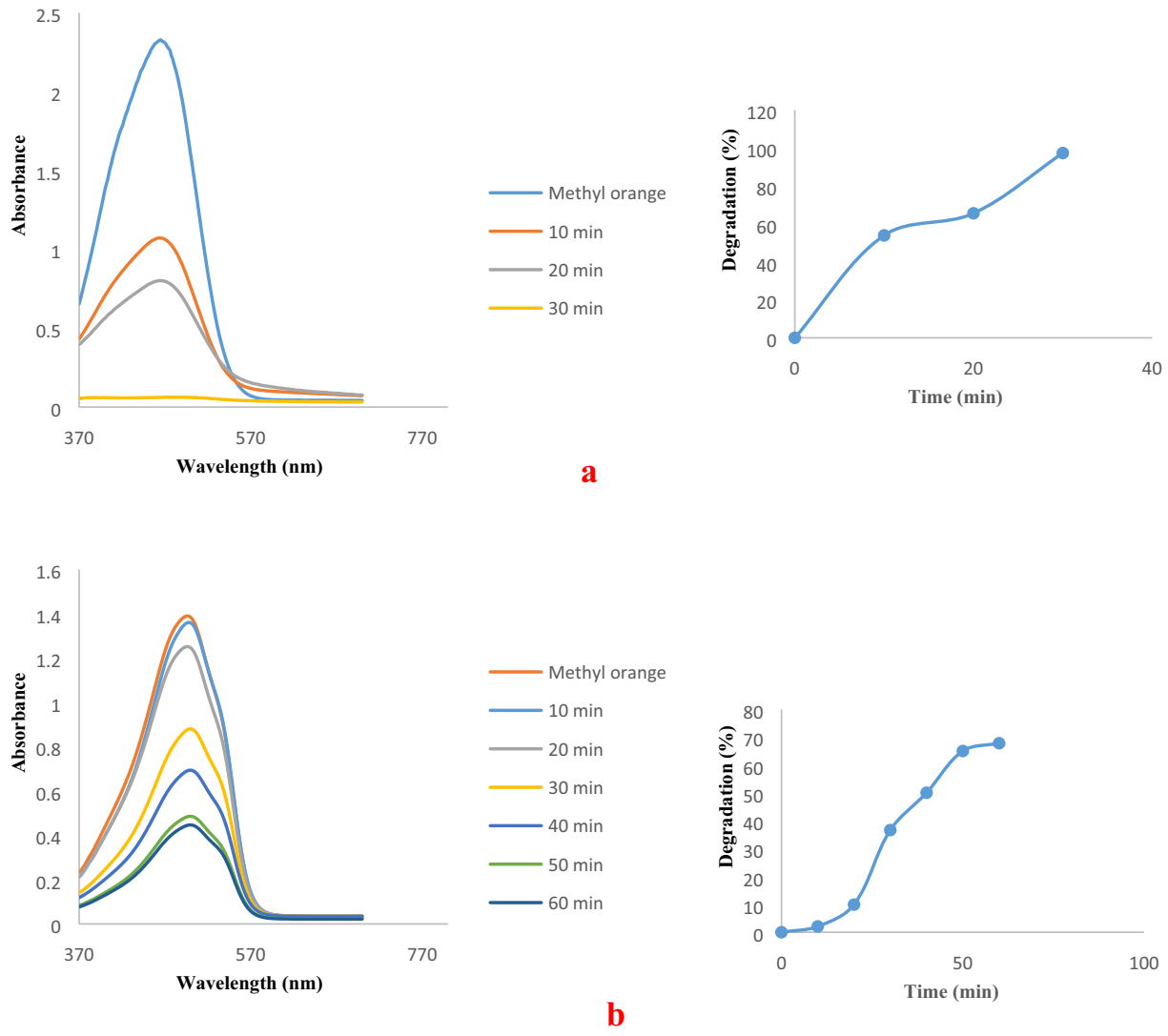

Fig. 14 UV–visible spectra of (a) MO catalytic decolourisation in the presence of FCP/PdNPs as spherical, and (b) MO catalytic decolourisation in the presence of FCP/PdNPs as rod shape.

caria and angioedema (Modirshahla et al., 2007). Thus, it is crucial for tartrazine azo dye to be treated before being released into the environment. Several approaches have been demonstrated for tartrazine removal of degradation, such as ozonation, electrochemical oxidation, photo Fenton oxidation, UV/HO, photolytic, photocatalytic oxidation, adsorption and biological treatments (Shu and Huang, 1995; Jain et al., 2003; Oancea and Meltzer, 2013; Dos Santos et al., 2014; Darwish et al., 2016). To the best of our knowledge the decolourisation of tartrazine at room temperature has been largely overlooked and has never been studied using functionalized cellulose-Preyssler-PdNPs as green nanobiocomposites. The decolourisation of tartrazine at room temperature, performed as a test reaction to estimate the catalytic activity of the FCP/PdNPs and the processes were checked by UV–vis analysis in several time intervals. The degradation efficiency (%) of tartrazine was calculated by the following equation:

$$\text{Degradation } (\%) = (C_0 - C)/C_0 \times 100 \quad (1)$$

where C_0 (mg/L) is the initial concentration and C (mg/L) is the concentration of tartrazine at reaction time. Also for further studies we have investigated the application of the catalyst for decolorization of two other azo dyes. Our findings showed that this catalyst is very active for decolorization of methyl orange (MeO) and Rodamine B (RB) as well as tartazine. Figs. 13–15 show typical time-dependent UV–Vis spectrum of these dyes during treating with the catalysts in spherical and rod shapes of PdNSs. The rate of decolorization was recorded in accordance with the change in the intensity of absorption peak in visible region.

Fig. 13a and b illustrates, the total absorption of tartrazine decreased to approx. 70% decolourisation after roughly 25 min in the presence of spherical PdNPs and 47.5% using rod shapes of PdNPs for 60 min. As can be seen from this figure, before reaction (t = 0), the absorption spectrum of tartrazine dye was characterized by one band in visible region which its maximum absorption at 428 nm. This band in the visible region was associated with the chromophore-

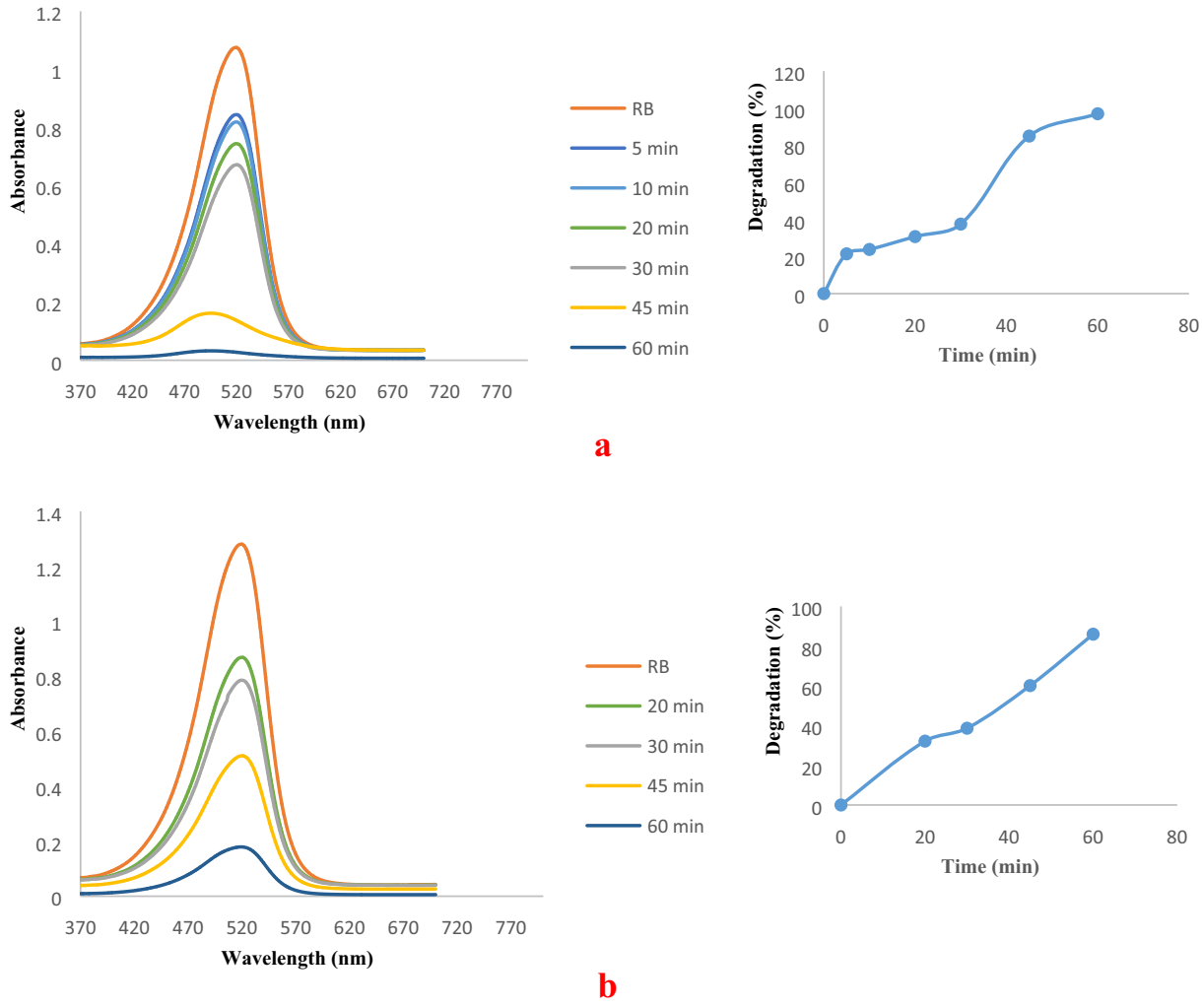

Fig. 15 UV–visible spectra of (a) MB catalytic decolourisation in the presence of FCP/PdNPs as spherical, and (b) MB catalytic decolourisation in the presence of FCP/PdNPs as rod shape.

containing azo linkage. The disappearance of the absorbance peak at 428 nm with the time was due to the fragmentation of the azo links by catalyst. The π electrons of tartazine can coordinate with the active site of Pd NPs on the surface, and adsorbs on the FCP/PdNPs catalyst, and then degradation occurs on the surface.

The UV–Vis analysis for the decolorization of MeO is shown in Fig. 14a and b. Almost 98% and 68% decolorization was observed when experiments were carried out using spherical and rod shapes of PdNPs for 30 and 60 min, respectively. Absorption peak of RB was also diminished, indicating, degradation of the corresponding dye (Fig. 15a and b). In the presence of spherical and rod shapes of the PdNSs, almost 97% and 86% decolorization was observed for 60 min, respectively. It is known that many catalytic processes occur at the perimeter interface around the nanoparticles where the fraction of step sites increases significantly with decreasing particle size (Bratlie et al., 2007). Here, spherical Pd NPs were found to have degraded azo dyes faster than Pd nano rods. The particles at connecting interfaces of rods are much less exposed to the surface resulting in decreased numbers of low coordinated sites compared to the spherical Pd nanoparticles, which have all sites exposed as surface and available for coordination of π electrons of azo dyes. Also, the larger size of Pd NRds provides low surface coverage in the reaction mixture, whereas for Pd NPs their smaller size and homogenous distribution provides increased numbers of contact sites for the reactant molecules within the reaction medium.

3.4. Reusability of the catalyst

In the recycling study, this catalyst could be recovered and reused many times without any loss of catalytic activity. This result clearly indicates that the catalyst is quite stable and recyclable without a significant loss of catalytic activity after 4 cycles (2–3%).

4. Conclusion

In summary, this work provides a simple and fast method for in-situ catalytic synthesis of Pd nanoparticles on the surface of the functionalized microcrystalline cellulose/Preyssler HPA to prepare a green nanobiocomposite as an eco-friendly heterogeneous catalyst. The possibility of bringing together inorganic polymers, nanoparticles and cellulose matrices opens a new

field for future applications, where the design and engineering of natural based multifunctional polymers will be privileged.

The most important conclusions are listed below.

- New and green polymeric biocomposites synthesized using cellulose and Preyssler heteropolyacid.
- Biocomposites produced nanobiocomposites via in-situ catalytic synthesis of Pd nanostructures on the surface.
- Pd nanostructures formed on the biocomposites surface in spherical and rod shapes.
- Fast and locally synthesis of Pd nanoparticles occurred in 2–4 min.
- The loading of Preyssler and pH could control the size and morphology of the decorated Pd nanostructures on the surface as well as their formation speed.
- SEM and TEM images showed that by increasing the Preyssler loading from 8 to 50 wt%, spherical Pd nanostructures changed to nanorods.
- SEM micrographs showed the PdNPs on the surface are cloudy and spherical at the low Preyssler loadings, and changed to rod shaped by increasing the Preyssler loading.
- TEM images revealed the average size of 5–50 nm for PdNPs.
- Nanobiocomposites exhibited high surface catalytic activity in decolorization of tartrazine, methyl orange and rodamine B.
- The nanocatalysts proved to be a recoverable catalyst without a significant loss of catalytic activity after 4 cycles (2–3%).

Declaration of Competing Interest

The authors declare that they have no known competing financial interests or personal relationships that could have appeared to influence the work reported in this paper.

Acknowledgements

The authors are highly thankful from Islamic Azad University Mashhad Branch, and Laboratory of Green Chemistry, LUT Chemtech, at Lappeenranta University of Technology for offering all facilities and instruments as well as TEM, SEM, XRD, TGA and BET analysis to complete this project.

References

Ayati, A., Ahmadpour, A., Bamoharram, F.F., Heravi, M.M., Sillanpää, M., 2012. Rate redox-controlled green photosynthesis of gold nanoparticles using H 3 + xPMo 12-xV xO 40. Gold Bull. 45, 145–151. https://doi.org/10.1007/s13404-012-0058-5.

Ayati, A., Ahmadpour, A., Bamoharram, F.F., Tanhaei, B., Mänttäri, M., Lahtinen, M., Sillanpää, M., 2014. Novel Au NPs/Preyssler acid/TiO2 nanocomposite for the photocatalytic removal of azo dye. Sep. Purif. Technol. 133, 415–420. https://doi.org/10.1016/j.seppur.2014.06.055.

Ayati, A., Heravi, M.M., Daraie, M., Tanhaei, B., Bamoharram, F.F., Sillanpaa, M., 2016a. H3PMo12O40 immobilized chitosan/Fe3O4 as a novel efficient, green and recyclable nanocatalyst in the synthesis of pyrano-pyrazole derivatives. J. Iran. Chem. Soc. 13, 2301–2308. https://doi.org/10.1007/s13738-016-0949-0.

Ayati, A., Tanhaei, B., Bamoharram, F.F., Ahmadpour, A., Maydannik, P., Sillanpää, M., 2016b. Photocatalytic degradation of nitrobenzene by gold nanoparticles decorated polyoxometalate immobilized TiO2 nanotubes. Sep. Purif. Technol. 171, 62–68. https://doi.org/10.1016/j.seppur.2016.07.015.

Ayati, A., Tanhaei, B., Lahtinen, M., Bamoharram, F.F., Sillanpää, M., 2015. Phosphotungstic acid (PTA) in the synthesis of 3D CdS superstructures by diffusion assisted hydrothermal method. Adv. Powder Technol. 26, 1495–1503. https://doi.org/10.1016/j.apt.2015.08.008.

Azetsu, A., Koga, H., Isogai, A., Kitaoka, T., 2011. Synthesis and catalytic features of hybrid metal nanoparticles supported on cellulose nanofibers. Catalysts 1, 83–96. https://doi.org/10.3390/catal1010083.

B. Pinto, R.J., C., M., Pascoal, C., Trindade, T., 2012. Composites of Cellulose and Metal Nanoparticles, in: Nanocomposites – New Trends and Developments. 10.5772/50553.

Bamoharram, F., Kadkhodaei, S., Ayati, A., Baharara, J., Heravi, M., 2014. Mono-substituted molybdenium preyssler heteropolyacid: an ecofriendly photocatalyst for the syntheses of gold nanoparticles in solution and titanium dioxide surface with excellent photoactivity in combination with titanium dioxide. Curr. Nanosci. 11, 80–86. https://doi.org/10.2174/15734137106661407081733321.

Bamoharram, F.F., Heravi, M.M., Roshani, M., Jahangir, M., Gharib, A., 2006. Preyssler catalyst, [NaP5W30O110] 14-: a green, efficient and reusable catalyst for esterification of salicylic acid with aliphatic and benzylic alcohols. Appl. Catal. A Gen. 302, 42–47. https://doi.org/10.1016/j.apcata.2005.12.021.

Baruah, S., Dutta, J., 2009. pH-dependent growth of zinc oxide nanorods. J. Cryst. Growth 311, 2549–2554. https://doi.org/10.1016/j.jcrysgro.2009.01.135.

Bhardwaj, M., Paul, S., 2016. Palladium nanoparticles onto ethylenediamine functionalized silica-cellulose substrates [Pd(0)-EDA/SCs]: an efficient and sustainable approach for hydrogenation of nitroarenes and carbonyl compounds under mild conditions. J. Chem Arab. https://doi.org/10.1016/j.arabjc.2016.05.008.

Bratlie, K.M., Lee, H., Komvopoulos, K., Yang, P., Somorjai, G.A., 2007. Platinum nanoparticle shape effects on benzene hydrogenation selectivity. Nano Lett. 7, 3097–3101. https://doi.org/10.1021/nl0716000.

Chang, G., Luo, Y., Lu, W., Qin, X., Asiri, A.M., Al-Youbi, A.O., Sun, X., 2012. Ag nanoparticles decorated polyaniline nanofibers: synthesis, characterization, and applications toward catalytic reduction of 4-nitrophenol and electrochemical detection of H 2O 2 and glucose. Catal. Sci. Technol. 2, 800–806. https://doi.org/10.1039/c2cy00454b.

Chen, F., Huang, M., Li, Y., 2014. Synthesis of a novel cellulose microencapsulated palladium nanoparticle and its catalytic activities in Suzuki-Miyaura and mizoroki-heck reactions. Ind. Eng. Chem. Res. 53, 8339–8345. https://doi.org/10.1021/ie4038505.

Cheng, N., Tian, J., Liu, Q., Ge, C., Qusti, A.H., Asiri, A.M., Al-Youbi, A.O., Sun, X., 2013. Au-nanoparticle-loaded graphitic carbon nitride nanosheets: Green photocatalytic synthesis and application toward the degradation of organic pollutants. ACS Appl. Mater. Interfaces 5, 6815–6819. https://doi.org/10.1021/am401802r.

Cheong, S., Watt, J.D., Tilley, R.D., 2010. Shape control of platinum and palladium nanoparticles for catalysis. Nanoscale. https://doi.org/10.1039/c0nr00276c.

Cirtiu, C.M., Dunlop-Brière, A.F., Moores, A., 2011. Cellulose nanocrystallites as an efficient support for nanoparticles of palladium: application for catalytic hydrogenation and Heck coupling under mild conditions. Green Chem. 13, 288–291. https://doi.org/10.1039/c0gc00326c.

Darwish, M., Mohammadi, A., Assi, N., 2016. Microwave-assisted polyol synthesis and characterization of pvp-capped cds nanoparticles for the photocatalytic degradation of tartrazine. Mater. Res.

Bull. 74, 387–396. https://doi.org/10.1016/j.materresbull.2015.11.002.

Djakovitch, L., Koehler, K., 2001. Heck reaction catalyzed by Pd-modified zeolites. J. Am. Chem. Soc. 123, 5990–5999. https://doi.org/10.1021/ja001087r.

Dos Santos, T.C., Zocolo, G.J., Morales, D.A., de Umbuzeiro, G.A., Zanoni, M.V.B., 2014. Assessment of the breakdown products of solar/UV induced photolytic degradation of food dye tartrazine. Food Chem. Toxicol. 68, 307–315. https://doi.org/10.1016/j.fct.2014.03.025.

Fortunati, E., Armentano, I., Zhou, Q., Iannoni, A., Saino, E., Visai, L., Berglund, L.A., Kenny, J.M., 2012a. Multifunctional bionanocomposite films of poly(lactic acid), cellulose nanocrystals and silver nanoparticles. Carbohydr. Polym. 87, 1596–1605. https://doi.org/10.1016/j.carbpol.2011.09.066.

Fortunati, E., Armentano, I., Zhou, Q., Puglia, D., Terenzi, A., Berglund, L.A., Kenny, J.M., 2012b. Microstructure and non-isothermal cold crystallization of PLA composites based on silver nanoparticles and nanocrystalline cellulose. Polym. Degrad. Stab., 2027–2036 https://doi.org/10.1016/j.polymdegradstab.2012.03.027.

Ganapathy, S., Fournier, M., Paul, J.F., Delevoye, L., Guelton, M., Amoureux, J.P., 2002. Location of protons in anhydrous keggin heteropolyacids H3PMo12O40 and H3PW12O40 by 1H{31P}/31P {1H} REDOR NMR and DFT quantum chemical calculations. J. Am. Chem. Soc. 124, 7821–7828. https://doi.org/10.1021/ja017848n.

Genovese, M., Lian, K., 2015. Polyoxometalate modified inorganic-organic nanocomposite materials for energy storage applications: a review. Curr. Opin. Solid State Mater. Sci. https://doi.org/10.1016/j.cossms.2014.12.002.

Guibal, E., 2005. Heterogeneous catalysis on chitosan-based materials: a review. Prog. Polym. Sci. https://doi.org/10.1016/j.progpolymsci.2004.12.001.

Hoffmann, F., Cornelius, M., Morell, J., Fröba, M., 2006. Silica-based mesoporous organic-inorganic hybrid materials. Angew. Chemie – Int. Ed. https://doi.org/10.1002/anie.200503075.

Irvin, C.W., Satam, C.C., Carson Meredith, J., Shofner, M.L., 2019. Mechanical reinforcement and thermal properties of PVA tricomponent nanocomposites with chitin nanofibers and cellulose nanocrystals. Compos. Part A Appl. Sci. Manuf. 116, 147–157. https://doi.org/10.1016/j.compositesa.2018.10.028.

Ito, H., Sakata, M., Hongo, C., Matsumoto, T., Nishino, T., 2018. Cellulose nanofiber nanocomposites with aligned silver nanoparticles. Nanocomposites 4, 167–177. https://doi.org/10.1080/20550324.2018.1556912.

Jain, R., Bhargava, M., Sharma, N., 2003. Electrochemical studies on a pharmaceutical azo dye: Tartrazine. Ind. Eng. Chem. Res. 42, 243–247. https://doi.org/10.1021/ie020228q.

Jebali, Z., Granados, A., Nabili, A., Boufi, S., do Rego, A.M.B., Majdoub, , Vallribera, H.A., 2018. Cationic cellulose nanofibrils as a green support of palladium nanoparticles: catalyst evaluation in Suzuki reactions. Cellulose 25, 6963–6975. https://doi.org/10.1007/s10570-018-2085-8.

Khadempir, S., Ahmadpour, A., Hamed Mosavian, M.T., Ashraf, N., Bamoharram, F.F., Fernández-Pacheco, R., De La Fuente, J.M., Mitchell, S.G., 2016. Mechanistic insights into the activation process in electrocatalytic ethanol oxidation by phosphomolybdic acid-stabilised palladium(0) nanoparticles (PdNPs@PMo12). RSC Adv. 6, 5359–5366. https://doi.org/10.1039/c5ra22698h.

Khadempir, S., Ahmadpour, A., Hamed Mosavian, M.T., Ashraf, N., Bamoharram, F.F., Mitchell, S.G., De La Fuente, J.M., 2015. A polyoxometalate-assisted approach for synthesis of Pd nanoparticles on graphene nanosheets: synergistic behaviour for enhanced electrocatalytic activity. RSC Adv. 5, 24319–24326. https://doi.org/10.1039/c5ra01084e.

Klemm, D., Heublein, B., Fink, H.P., Bohn, A., 2005. Cellulose: Fascinating biopolymer and sustainable raw material. Angew. Chemie – Int. Ed. https://doi.org/10.1002/anie.200460587.

Klingelhöfer, S., Heitz, W., Greiner, A., Oestreich, S., Förster, S., Antonietti, M., 1997. Preparation of palladium colloids in block copoloymer micelles and their use for the catalysis of the heck reaction. J. Am. Chem. Soc. 119, 10116–10120. https://doi.org/10.1021/ja9714604.

Li, H., Chang, G., Zhang, Y., Tian, J., Liu, S., Luo, Y., Asiri, A.M., Al-Youbi, A.O., Sun, X., 2012. Photocatalytic synthesis of highly dispersed Pd nanoparticles on reduced graphene oxide and their application in methanol electro-oxidation. Catal. Sci. Technol. 2, 1153–1156. https://doi.org/10.1039/c2cy20099f.

Li, Y., Xu, L., Xu, B., Mao, Z., Xu, H., Zhong, Y., Zhang, L., Wang, B., Sui, X., 2017. Cellulose sponge supported palladium nanoparticles as recyclable cross-coupling catalysts. ACS Appl. Mater. Interfaces 9, 17155–17162. https://doi.org/10.1021/acsami.7b03600.

Li, Y.-Y., Wang, B., Ma, M.-G., Wang, B., 2018. Review of recent development on preparation, properties, and applications of cellulose-based functional materials. Int. J. Polym. Sci. 2018, 1–18. https://doi.org/10.1155/2018/8973643.

Liang, S., Guo, X., Feng, N., Tian, Q., 2010. Isotherms, kinetics and thermodynamic studies of adsorption of Cu 2+ from aqueous solutions by Mg 2+/K + type orange peel adsorbents. J. Hazard. Mater. 174, 756–762. https://doi.org/10.1016/j.jhazmat.2009.09.116.

Lim, B., Xia, Y., 2011. Metal nanocrystals with highly branched morphologies. Angew. Chemie – Int. Ed. https://doi.org/10.1002/anie.201002024.

Liu, H., Wang, D., Shang, S., Song, Z., 2011. Synthesis and characterization of Ag-Pd alloy nanoparticles/carboxylated cellulose nanocrystals nanocomposites. Carbohydr. Polym. 83, 38–43. https://doi.org/10.1016/j.carbpol.2010.07.019.

Liu, S., Tian, J., Wang, L., Luo, Y., Sun, X., 2012. One-pot synthesis of CuO nanoflower-decorated reduced graphene oxide and its application to photocatalytic degradation of dyes. Catal. Sci. Technol. 2, 339–344. https://doi.org/10.1039/c1cy00374g.

Lu, W., Qin, X., Li, H., Asiri, A.M., Al-Youbi, A.O., Sun, X., 2013. One-step hydrothermal synthesis of ag nanoparticle decorated submicrometer-scale spherical AgBr colloids: a highly efficient visible light plasmonic photocatalyst for degradation of organic dyes. Part. Part. Syst. Char. 30, 67–71. https://doi.org/10.1002/ppsc.201200033.

Mishra, R.K., Anis, A., Mondal, S., Dutt, M., Banthia, A.K., 2009. Reparation and characterization of amidated pectin based polymer electrolyte membranes. Chin. J. Polym. Sci. 27, 639. https://doi.org/10.1142/s0256767909004333.

Modirshahla, N., Behnajady, M.A., Kooshaiian, S., 2007. Investigation of the effect of different electrode connections on the removal efficiency of Tartrazine from aqueous solutions by electrocoagulation. Dye. Pigment. 74, 249–257. https://doi.org/10.1016/j.dyepig.2006.02.006.

Nabi, S.A., Naushad, M., 2008. Synthesis, characterization and analytical applications of a new composite cation exchanger cellulose acetate-Zr(IV) molybdophosphate. Colloids Surfaces A Physicochem. Eng. Asp. 316, 217–225. https://doi.org/10.1016/j.colsurfa.2007.09.005.

Oancea, P., Meltzer, V., 2013. Photo-Fenton process for the degradation of Tartrazine (E102) in aqueous medium. J. Taiwan Inst. Chem. Eng. 44, 990–994. https://doi.org/10.1016/j.jtice.2013.03.014.

Opanasenko, M., Štěpnička, P., Čejka, J., 2014. Heterogeneous Pd catalysts supported on silica matrices. RSC Adv. https://doi.org/10.1039/c4ra11963k.

Polshettiwar, V., Molnár, Á., 2007. Silica-supported Pd catalysts for Heck coupling reactions. Tetrahedron 63, 6949–6976. https://doi.org/10.1016/j.tet.2007.04.023.

Rajender Reddy, K., Kumar, N.S., Surendra Reddy, P., Sreedhar, B., Lakshmi Kantam, M., 2006. Cellulose supported palladium(0) catalyst for Heck and Sonogashira coupling reactions. J. Mol.

Catal. A: Chem. 252, 12–16. https://doi.org/10.1016/j.molcata.2006.02.024.

Ren, Y., Wang, M., Chen, X., Yue, B., He, H., 2015. Heterogeneous catalysis of polyoxometalate based organic-inorganic hybrids. Materials (Basel). https://doi.org/10.3390/ma8041545.

Rezayat, M., Blundell, R.K., Camp, J.E., Walsh, D.A., Thielemans, W., 2014. Green one-step synthesis of catalytically active palladium nanoparticles supported on cellulose nanocrystals. ACS Sustain. Chem. Eng. 2, 1241–1250. https://doi.org/10.1021/sc500079q.

Sanchez, C., Belleville, P., Popall, M., Nicole, L., 2011. Applications of advanced hybrid organic-inorganic nanomaterials: from laboratory to market. Chem. Soc. Rev. 40, 696–753. https://doi.org/10.1039/c0cs00136h.

Sheldon, R.A., Van Bekkum, H., 2007. Fine Chemicals through Heterogeneous Catalysis, Fine Chemicals through Heterogeneous Catalysis. John Wiley & Sons. https://doi.org/10.1002/9783527612963.

Shu, H.Y., Huang, C.R., 1995. Degradation of commercial azo dyes in water using ozonation and UV enhanced ozonation process. Chemosphere 31, 3813–3825. https://doi.org/10.1016/0045-6535(95)00255-7.

Tanaka, T., 2006. Reproductive and neurobehavioural toxicity study of tartrazine administered to mice in the diet. Food Chem. Toxicol. 44, 179–1178.

Tanhaei, B., Ayati, A., Bamoharram, F.F., Sillanpää, M., 2017. Magnetic EDTA functionalized preyssler cross linked chitosan nanocomposite for adsorptive removal of Pb(II) ions. Clean – Soil Air Water 45. https://doi.org/10.1002/clen.201700328.

Tripathi, B.P., Shahi, V.K., 2011. Organic-inorganic nanocomposite polymer electrolyte membranes for fuel cell applications. Prog. Polym. Sci. https://doi.org/10.1016/j.progpolymsci.2010.12.005.

Viswanathan, N., Meenakshi, S., 2010. Development of chitosan supported zirconium(IV) tungstophosphate composite for fluoride removal. J. Hazard. Mater. 176, 459–465. https://doi.org/10.1016/j.jhazmat.2009.11.051.

Wang, Y., He, J., Liu, C., Chong, W.H., Chen, H., 2015. Thermodynamics versus kinetics in Nanosynthesis. Angew. Chemie – Int. Ed. 54, 2022–2051. https://doi.org/10.1002/anie.201402986.

Wight, A.P., Davis, M.E., 2002. Design and preparation of organic–inorganic hybrid catalysts. Chem. Rev. 102, 3589–3614. https://doi.org/10.1021/cr010334m.

Wu, X., Lu, C., Zhang, W., Yuan, G., Xiong, R., Zhang, X., 2013. A novel reagentless approach for synthesizing cellulose nanocrystal-supported palladium nanoparticles with enhanced catalytic performance. J. Mater. Chem. A 1, 8645–8652. https://doi.org/10.1039/c3ta11236e.

Xu, Y., Zhang, L., Cui, Y., 2008. Catalytic performance of cellulose supported palladium complex for Heck reaction in water. J. Appl. Polym. Sci. 110, 2996–3000. https://doi.org/10.1002/app.28655.

Yang, J., Yu, J., Fan, J., Sun, D., Tang, W., Yang, X., 2011. Biotemplated preparation of CdS nanoparticles/bacterial cellulose hybrid nanofibers for photocatalysis application. J. Hazard. Mater. 189, 377–383. https://doi.org/10.1016/j.jhazmat.2011.02.048.

Yu, H.Y., Yang, X.Y., Lu, F.F., Chen, G.Y., Yao, J.M., 2016. Fabrication of multifunctional cellulose nanocrystals/poly(lactic acid) nanocomposites with silver nanoparticles by spraying method. Carbohydr. Polym. 140, 209–219. https://doi.org/10.1016/j.carbpol.2015.12.030.

Zhang, D.Y., Duan, M.H., Yao, X.H., Fu, Y.J., Zu, Y.G., 2016. Preparation of a novel cellulose-based immobilized heteropoly acid system and its application on the biodiesel production. Fuel 172, 293–300. https://doi.org/10.1016/j.fuel.2015.12.020.

Zhang, K., Shen, M., Liu, H., Shang, S., Wang, D., Liimatainen, H., 2018. Facile synthesis of palladium and gold nanoparticles by using dialdehyde nanocellulose as template and reducing agent. Carbohydr. Polym. 186, 132–139. https://doi.org/10.1016/j.carbpol.2018.01.048.

Zhou, P., Wang, H., Yang, J., Tang, J., Sun, D., Tang, W., 2012. Bacteria cellulose nanofibers supported palladium(0) nanocomposite and its catalysis evaluation in heck reaction. Ind. Eng. Chem. Res. 51, 5743–5748. https://doi.org/10.1021/ie300395q.

Zou, J., Iyer, K.S., Raston, C.L., 2012. Pd-sodium carboxymethyl cellulose nanocomposites display a morphology dependent response to hydrogen gas. Green Chem. 14, 906–908. https://doi.org/10.1039/c2gc16456f.